symmetry

Article

Accurate Electromagnetic Force Analysis of Offshore Wind Power Transformer Windings Based on Fractional Order Lumped Parameter Model

Hui Zhong , Yuheng Zuo *, Runze Wang, Li Zhang and Xiaoshan Ouyang

School of Electrical Engineering, Shandong University, Jinan 250061, China; zhonghui@sdu.edu.cn (H.Z.); 202034702@mail.sdu.edu.cn (R.W.); zhleee@sdu.edu.cn (L.Z.); 202214628@mail.sdu.edu.cn (X.O.)
* Correspondence: 202114620@mail.sdu.edu.cn

Abstract: Accurate calculation of the electromagnetic force distribution of transformer windings under different loads and fault conditions is of great significance for transformer maintenance, condition evaluation and life prediction. Due to the influence of offshore wind power systems, offshore wind power transformers have high harmonic content and large changes in load rates, which can easily cause the coil destabilization, winding deformation or even damage because of the uneven distribution of the electromagnetic force. To improve the accuracy of electromagnetic force calculation, this paper proposes a fractional order numerical method. First, a three-dimensional axisymmetric transformer model and a symmetrical lumped parameter equivalent circuit model are established, respectively, based on field-circuit coupling. Second, the fractional order approximation of circuit components is realized by using the improved Oustaloup filter. In the fractional order model, the transformer is replaced by the lumped parameter equivalent circuit model. Third, as in the calculation process for integer order electromagnetic force, the integer order current has a large error, and the current waveform does not match the actual power frequency. The fractional order current and electromagnetic force at the 0.9 order are closer to the rated value. Finally, the effects of different load rates, three-phase short circuits and harmonic conditions are studied with the fractional order model. Compared with the traditional integer order finite element electromagnetic model, the fractional order equivalent circuit model established in this paper is more accurate and suitable for electromagnetic force calculation. The proposed method is significant for the structural design and state detection of transformers and also could be applied in the analysis of other dry-type transformers.

Keywords: offshore wind power transformer; fractional order; electromagnetic force; parameter circuit; finite element method

Citation: Zhong, H.; Zuo, Y.; Wang, R.; Zhang, L.; Ouyang, X. Accurate Electromagnetic Force Analysis of Offshore Wind Power Transformer Windings Based on Fractional Order Lumped Parameter Model. *Symmetry* **2023**, *15*, 1768. https://doi.org/10.3390/sym15091768

Academic Editor: Calogero Vetro

Received: 22 August 2023
Revised: 12 September 2023
Accepted: 14 September 2023
Published: 15 September 2023

1. Introduction

The offshore wind power transformer is an important item that connects the offshore wind power generator set and the power network. Because of the high humidity and salt spray in the marine environment, the operating conditions are not stable enough; there can be more fault states such as overload, short circuits, etc., which would produce an uneven distribution of electromagnetic force of windings and cause winding deformation, insulation damage, transformer scrapping, or even system collapse [1–3]. Nowadays, with the increasing application of power electronic devices in double-fed wind generators, increasing the harmonics causes a significant increase in transformer winding stress [4]. By accurately calculating the electromagnetic force in the winding, the operating conditions can be quickly determined to ensure the safety and stability of the transformer.

In recent years, scholars have conducted extensive research on the analysis of electromagnetic force and stress characteristics of transformers. The authors of [5] established a field-circuit coupling model to calculate the axial electromagnetic force of a winding and proposed dual frequency characteristics of an axial short-circuit electromagnetic force. A circuit-magnetic field-solid mechanics multi-physics coupling model was built in [6], and the influence of transformer stress characteristics on the change in winding mechanical conditions was studied. By combining the model with vibration signal measurement, the operating conditions of transformer windings were quickly detected. The authors of [7] made a three-dimensional multilayer transformer model of a transformer based on magnetic field-solid mechanics coupling, and simulated short-circuit electromagnetic force and found that the middle layer of the winding was subjected to larger radial electromagnetic force, while the layers at both ends were subjected to larger axial electromagnetic force. The influence of the short-circuit impedance of a three-phase power transformer on the cumulative effect of the electromagnetic force was evaluated in [8] by a finite element analysis model.

Due to the high cost and destructive nature of short-circuit impact tests of transformers, the simulation calculation method is widely used to analyze the electromagnetic force. The lumped parameter equivalent circuit model is used in simulation calculations because the model is simple and the computation is convenient. Authors of [9] studied the time-domain mathematical model of oscillating waves with capacitance and inductance matrix parameters, and found that the variation of capacitance parameters under an axial displacement fault had a significant effect on the oscillating waves. Authors of [10] analyzed the transformer winding characteristics and obtained a node voltage response. Authors of [11] studied the variation trend of sweep frequency impedance curves when short-circuit faults occurred on different windings, and analyzed the influence of short-circuit faults within different windings on sweep frequency impedance curves. The sweep frequency impedance curve showed obvious change under a short-circuit fault.

Since capacitors and inductors are essentially fractional order, the integer order capacitance and inductance parameters used in traditional transformer models can no longer accurately describe the characteristics of offshore wind power transformers [12]. Jonscher pointed out that the capacitive reactance form of integer order capacitance violated the fractional order characteristics of dielectric materials [13]. Under the study of H. M. Srivastava, fractional calculus began to become an independent and complete discipline [14]. The authors of [15] measured the orders of fractional capacitance in different dielectrics by experiment in 1994. A dual impedance converter based on fractional order inductance and capacitance was proposed in [16], which transmitted the complex impedance source of any frequency to two frequency loads through a fractional order inductance and two fractional order capacitances. Authors of [17] studied four passive synthesis methods for a fractal order circuit model, which described the physical significance of components better and improved the accuracy of the model. A new operator called conformable derivative in the Caputo sense was proposed in [18] and derived the solution for the two-parameter operator of a circuit containing two supercapacitors. The operator could be extended for circuits containing any number of elements.

With the development of fractional order theory, modeling and simulation technology and control strategies for electrical equipment have been widely developed. A low-pass virtual filter for wind energy conversion systems was proposed in [19] to smooth the output power; the high-frequency term was restrained, and the wind power fluctuation was mitigated with the proposed virtual filter. The authors of [20] proposed an improved fractional-order sliding mode controller to optimize the adaptive fractional-order sliding-mode disturbance observer and realized the theoretical frequency regulation of a hybrid wind–diesel-based power system. The proposed resilient fractional-order nonlinear controller was capable of countering unknown or uncertain system disturbances. A fractional-order recurrent neural network was proposed in [21] to realize an optimal maneuvering decision-making algorithm, which improved the convergence rate and reduced the optimization error by the fractional-order parameter.

In this paper, the fractional order characteristics of circuit components are well described by using a fractional order filter, and a fractional order-lumped parameter-equivalent circuit model is proposed to realize the fast and accurate calculation of the electromagnetic force. A 35 kV offshore wind power dry-type transformer is taken as the research object, and the three-dimensional axisymmetric geometric model of the transformer is established by the finite element method. Based on the field-circuit coupling method, the results of the fractional order numerical method are compared with the traditional integer order finite element method for the calculation of electromagnetic force of the transformer winding. The accuracy and correctness of the fractional order model are verified. This new stress calculation method provides guidance for the operating condition evaluation and process design of transformers.

2. Finite Element Model and Simulation

An existing 35 kV offshore wind power transformer is taken as the research object in this paper [22]. Based on electromagnetic coupling theory, a finite element simulation model of the wind power transformer is established. The transformer has a three-phase symmetrical structure; it uses epoxy resin as the insulation material, the high- and low-voltage windings are a segmented structure, and the insulation class is F. The transformer parameters are shown in Table 1.

Table 1. Parameters of dry-type transformer.

Parameters	Value	Parameters	Value
rated capacity	8000 kVA	rated frequency	50 Hz
rated voltage	35 kV/6.3 kV	rated current	132 A/733 A
core height	2630 mm	core radius	240 mm
turns of high-voltage winding coil	399	turns of low-voltage winding coil	113
high-voltage winding segments	9	low-voltage winding segments	2
height of each part of high-voltage winding	130 mm	height of each part of low-voltage winding	680 mm
inner radius of high-voltage winding	440 mm	inner radius of low-voltage winding	283 mm
outer radius of high-voltage winding	555 mm	outer radius of low-voltage winding	370 mm

To simplify the calculation, the finite element model is set as follows:

1. Since the clamp, pad and base are directly ignored for almost having no influence on the leakage magnetic field, only the structural models of the core, winding and insulation are built in the model;
2. The iron core is regarded as a whole, and the influence between silicon steel sheets of the iron core is negligible;
3. The winding shape is simplified into a cylinder.

The three-dimensional finite element model of the transformer is shown in Figure 1.

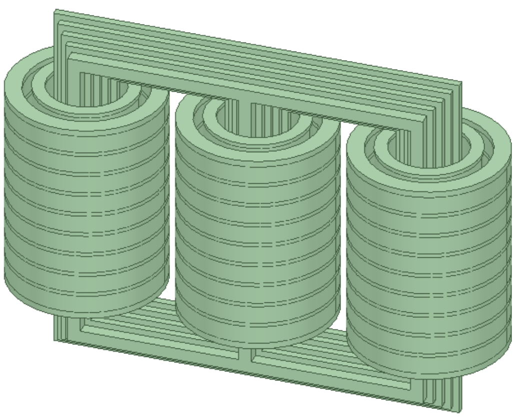

Figure 1. Three-dimensional simplified model of transformer.

The mesh division is finely processed to obtain more accurate simulation calculation results. The mesh results for the finite element model are shown in Figure 2.

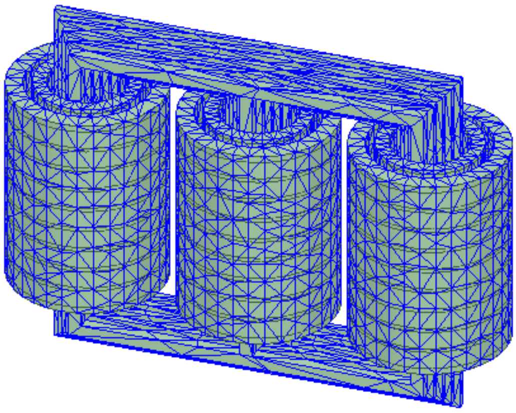

Figure 2. Three-dimensional simplified model of transformer.

As the transformer has a symmetrical structure, we can take one phase winding to simplify the calculation. By using the finite element transient solution type, the current of the A-phase winding is obtained as shown in Figure 3.

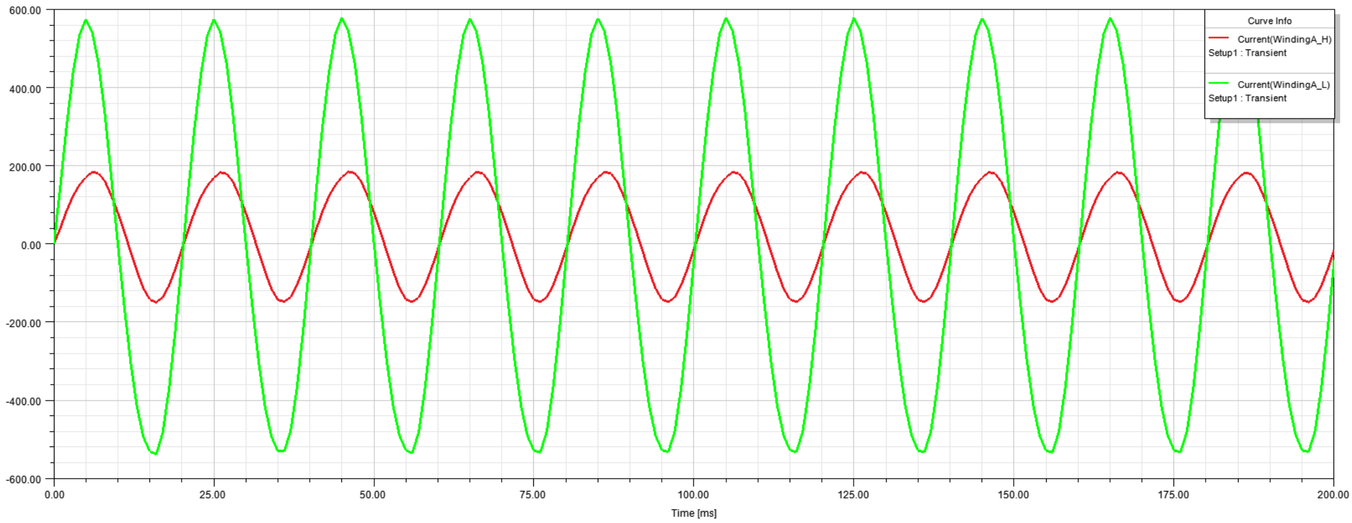

Figure 3. The current of A-phase winding.

The magnetic flux density of the A-phase winding is simulated by using the finite element method. The results are shown in Figure 4.

The magnetic flux density value for the high-voltage winding is smaller on the outer side of the winding and larger on the inner side of the winding. On the inner side of the high-voltage winding, the magnetic flux density is relatively small in the first and ninth segments, but relatively large in the second, third, fourth, sixth, seventh, and eighth segments. Overall, it is symmetrically distributed along the axial direction.

The magnetic flux density value of the low-voltage winding is larger on the outer side of the winding and smaller on the inner side of the winding. On the outer side of the low-voltage winding, the magnetic flux density is relatively small at both ends of the winding and relatively large in the middle of the winding. Overall, it is also symmetrically distributed along the axial direction.

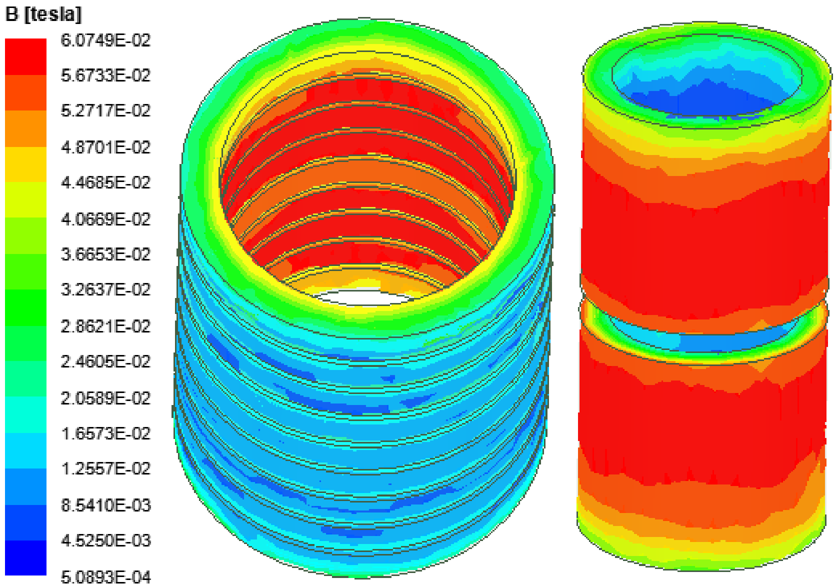

Figure 4. The magnetic flux density of A-phase winding.

The current density and magnetic flux density affect the electromagnetic force. According to the Maxwell equation, the magnetic field can be described by the following equation:

$$\nabla^2 A = -\mu J \tag{1}$$

The magnetic flux density can be derived as:

$$B_r = -\partial A/\partial z \tag{2}$$

$$B_z = -\partial(rA)/\partial r \tag{3}$$

$$B = \sqrt{B_r^2 + B_z^2} \tag{4}$$

where B is the magnitude of the magnetic flux density, B_r is the magnetic flux density in the radial direction, B_z is the magnetic flux density in the axial direction, A is the magnetic vector potential, μ is the magnetic permeability of the electromagnetic field.

The electromagnetic volume force can be expressed by the Lorentz law:

$$f = J \times B \tag{5}$$

where f is the electromagnetic volume force, J is the volume current density, B is the magnetic flux density.

The electromagnetic force per unit volume and electromagnetic force magnitude of the A-phase winding is calculated by using the finite element field calculator. The results are shown in Figures 5 and 6.

The per-unit volume electromagnetic force of the winding is symmetrically distributed along the axial direction, just like the magnetic flux density. Since the direction of current between the low-voltage and high-voltage windings is opposite, the low-voltage winding is subjected to inward force, while the high-voltage winding is subjected to outward force. When the distribution of electromagnetic force in the winding changes, the winding may break down because of insufficient mechanical strength.

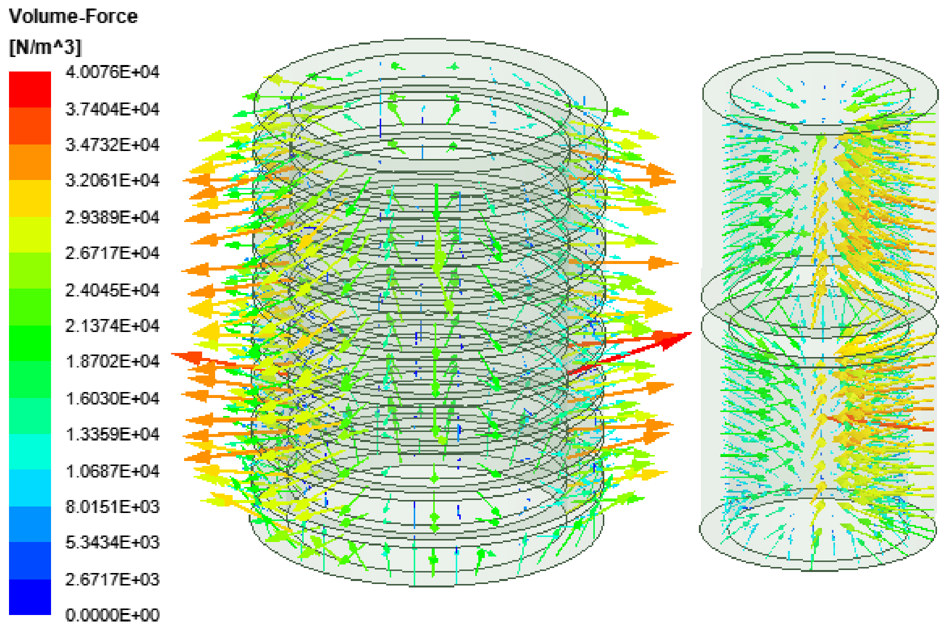

Figure 5. The electromagnetic force per unit volume of A-phase winding.

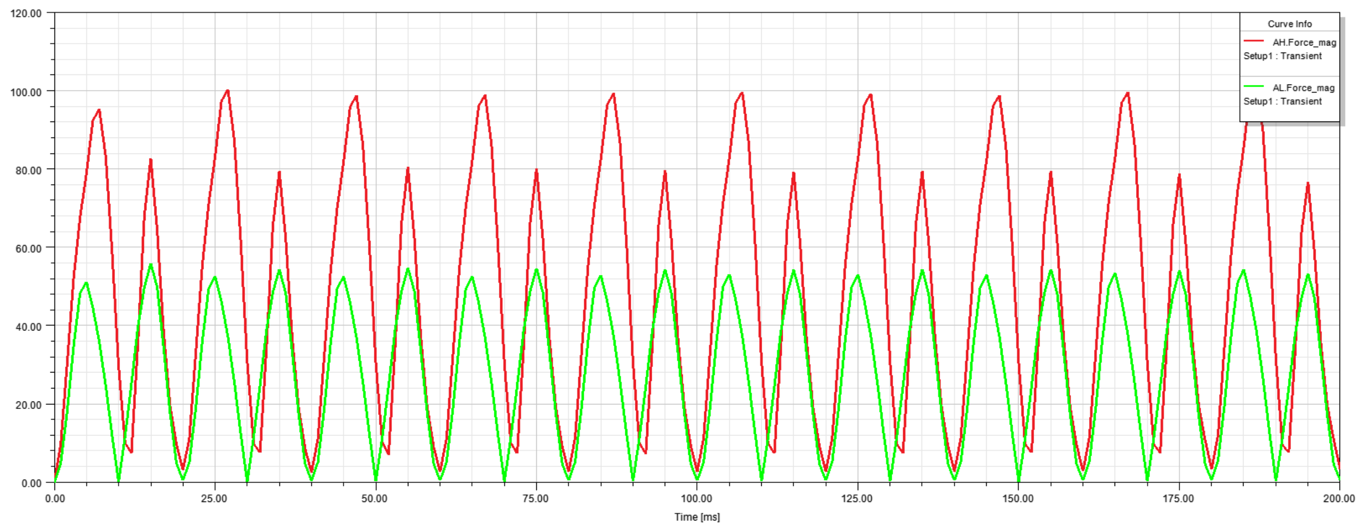

Figure 6. The electromagnetic force magnitude of A-phase winding.

The accuracy of the finite element method is offset by its complicated steps and long computational time while obtaining the distribution of electromagnetic force and the electromagnetic force magnitude of the winding. Therefore, it is necessary to establish an accurate circuit model to obtain high-accuracy calculation results of electromagnetic force values.

3. Parameters of Circuit Components

3.1. Resistance

In the lumped parameter circuit model, the resistance of each winding is the total of the resistance values of all turns in the coils connected in series, and the whole resistance expression is:

$$R = N\frac{\rho l}{S} \tag{6}$$

where R is the resistance of the coil, ρ is the conductivity of the conductor, l is the length of the coil in each segment of winding, S is the cross-segmental area of the coil, and N is the number of turns of the coil.

3.2. Inductance

The formula for calculating the coefficient of self-inductance of a coil containing an iron core is:

$$L = \frac{\mu S N^2}{l} \tag{7}$$

where L is the self-inductance of the coil, μ is the magnetic permeability of the media, S is the cross-segmental area of the coil, l is the length of the coil, and N is the number of turns of the coil.

The mutual inductance between two coils can be solved with the Neumann formula as in the following expression:

$$M_{12} = \frac{\varphi_{12}}{I_1} = \frac{\mu_0 N_1 N_2}{4\pi} \oint_{l_1} \oint_{l_2} \frac{dl_1 \cdot dl_2}{r} = M_{21} \tag{8}$$

where M_{12} and M_{21} are the mutual inductance between two coils, $\varnothing_{12}$ is the magnetic flux between two coils, I_1 is the current of one coil, μ_0 is the vacuum permeability, $N_1,\ N_2$ are the number of turns of two coils, r is the distance between the two coils, and $l_1,\ l_2$ are the average turn lengths of two coils, respectively.

Due to the uneven distribution of the magnetic field inside the transformer and the existence of the leakage field, the parameters calculated by the formula method are inaccurate [23]. This paper integrates an inductance matrix calculation module into the magnetic field solver to obtain the self- and mutual-inductance parameters of the winding. The current source is set as 1 A in the winding coil to calculate the inductance by using the magnetic field energy principle.

$$L = \frac{2W_m}{I^2} = \frac{\int_V HBdV}{I^2} \tag{9}$$

where W_m is the energy of the magnetic field generated in each segment of the winding, L is the self-inductance of each segment of the winding, I is the value of the winding current, H is the magnetic flux density in each segment of the winding, B is the magnetic induction intensity in each segment of the winding, V is the total spatial area of the winding model.

The expressions for the equivalent mutual inductance between the two windings are:

$$W_{12} = \frac{1}{2}\left(L_1 I_1^2 + L_2 I_2^2 + 2MI_1 I_2\right) \tag{10}$$

$$M = \frac{2W_{12} - L_1 I_1^2 - L_2 I_2^2}{2I_1 I_2} \tag{11}$$

where W_{12} is the magnetic field energy between two windings, M is the mutual inductance between two windings, L_1, L_2 are the self-inductance of two windings, respectively, and I_1, I_2 are the currents of two windings, respectively.

3.3. Capacitance

3.3.1. Coupling Capacitance between Windings

Since the transformer windings have nine segments in the high-voltage windings and two segments in the low voltage windings, the coupling capacitances between windings include coupling capacitances at the same horizontal position and at different horizontal positions. Figure 7 shows the coupling capacitance between high-voltage windings and low-voltage windings and the coupling capacitance between adjacent high-voltage windings.

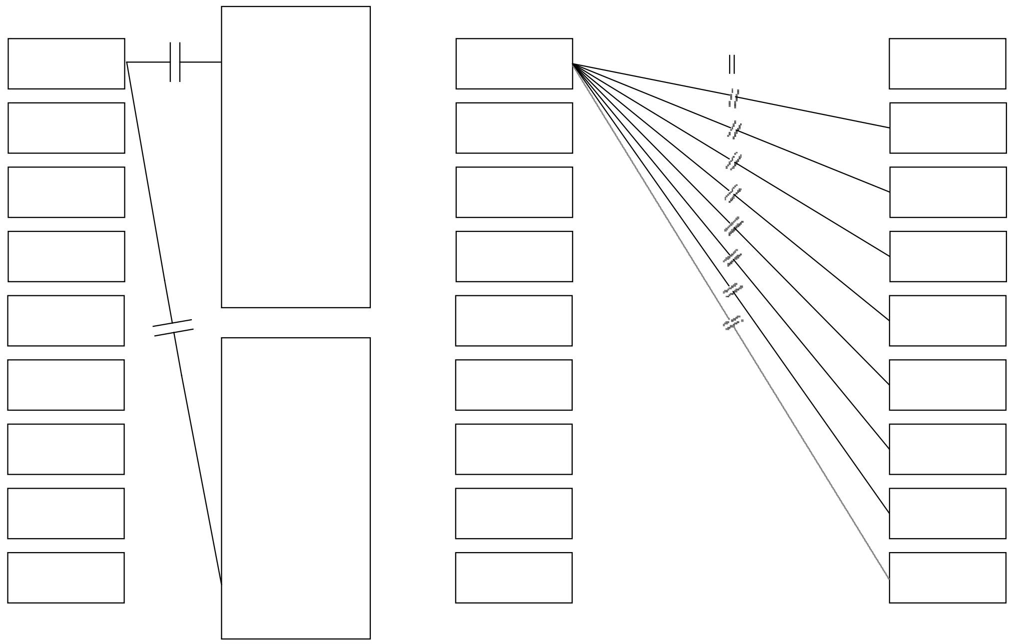

(**a**) (**b**)

Figure 7. Coupling capacitance between windings: (**a**) coupling capacitance between high voltage winding and low voltage winding, (**b**) coupling capacitance between adjacent high voltage windings.

The capacitance matrix calculation module is applied in the electrostatic field solver to solve the capacitance parameters of the winding. The voltage source is set as 1 V in the winding coil to calculate the capacitance by using the electric field energy principle.

$$C = \frac{2W_e}{U^2} == \frac{\int_V DEdV}{U^2} \tag{12}$$

where C is the coupling capacitance between windings, U is the voltage source, W_e is the electrostatic field energy, D is the flux density, and E is the electric field strength of the electrostatic field. The total electric field energy between the windings can be calculated from the finite element, and thus, the capacitance can be calculated. Some calculation values are shown in Table 2.

Table 2. Values of coupling capacitance between windings.

Winding Number	Capacitance Value/*pF*
A1-a1	144.73
A1-a2	59.781
A1-B1	48.546
A1-B2	50.256
A1-B3	50.846
A1-B4	51.192
A1-B5	50.623
A1-B6	48.523
A1-B7	46.530
A1-B8	44.944
A1-B9	42.834

3.3.2. Coupling Capacitance between Windings and Ground

The simulation model of capacitance between windings and ground is shown in Figure 8. Taking the A-phase windings as the example, we set the core, epoxy resin, low-voltage winding and the other eight segments of the high-voltage winding to zero potential. Equation (12) is used to calculate the value.

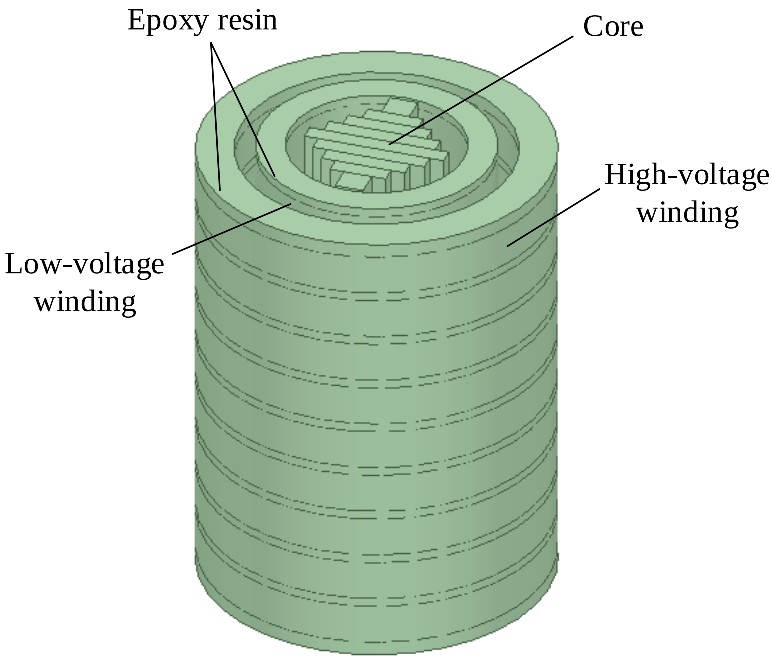

Figure 8. Simulation model of capacitance to ground.

Because the transformer is symmetrical, the values of capacitances between windings and ground in the B and C phases can be obtained by calculating values in the A phase. The calculation values are shown in Table 3.

Table 3. Values of coupling capacitance between windings and ground.

Winding Number	Capacitance Value/*pF*
a1-ground	34.210
a2-ground	38.857
A1-ground	32.232
A2-ground	33.291
A3-ground	34.228
A4-ground	35.510
A5-ground	37.149
A6-ground	38.098
A7-ground	38.547
A8-ground	39.002
A9-ground	39.172

3.3.3. Coupling Capacitance between Two Adjacent Series Windings

Since the transformer windings have nine segments along the axial direction in the high-voltage winding and two segments along the axial direction in the low-voltage winding, the effect of the coupling capacitance between two adjacent windings must be considered in the lumped parametric circuit model. The coupling capacitance between two adjacent series windings can be obtained from the parallel plate capacitor formula as shown in Equation (13).

$$C_W = \frac{\varepsilon_0 \varepsilon_r S}{d} \tag{13}$$

where C_W is the coupling capacitance between two adjacent series windings, ε_0 is the permittivity of vacuum, ε_r is the permittivity of epoxy resin, S is the cross-segmental area of winding, and d is the length of two adjacent windings.

Because the transformer is symmetrical, the parameters of the other two phases can be obtained by calculating the parameters of only one phase. The main electrical parameters of the winding under rated operating conditions are shown in Table 4.

Table 4. Electrical parameters of windings under rated operating conditions.

Parameters	***R*/Ω**	***L*/*mH***	C_W/*pF*
high-voltage winding	0.382	6.833	453.91
low-voltage winding	0.102	1.050	64.791

4. Fractional Order Circuit Model of Transformer

4.1. Fractional Order Arithmetic Implementation

The main methods of implementing fractional order operators in recent research are defining fractional order calculus formulae or constructing filters. The definition methods mainly include the GL definition method, RL definition method, and Caputo definition method. Based on the corresponding definition of fractional calculus, programs can be directly written for calculation. The definition method requires obtaining the specific expression of the objective function, and different sampling values can affect the accuracy of the calculation. In practical engineering applications, the specific objective function expression cannot be obtained in most cases. The filter method can perform fitting calculations for fractional order operators without obtaining the specific expression. In this paper, the fractional order operator is obtained by an improved Oustaloup filter in accordance with the research theory of Oustaloup [24].

The Oustaloup filter uses an integer order transfer function model to approximate a fractional order calculus operator. Assuming that the frequency band to be fitted is $[w_b, w_h]$, the standard form of the Oustaloup filter is as follows:

$$G(s) = K\prod_{k=1}^{N}\frac{s+w_k'}{s+w_k} \tag{14}$$

where $G(s)$ is the transfer function of the Oustaloup filter, N is the order of the filter, w_k' is zero, w_k is the pole, and K is the gain. The zero, pole and gain can be calculated as:

$$w_k' = w_b {w_u}^{(2k-1-\gamma)/N} \tag{15}$$

$$w_k = w_b {w_u}^{(2k-1+\gamma)/N} \tag{16}$$

$$K = w_h^{\gamma} \tag{17}$$

and

$$w_u = \sqrt{w_h/w_b} \tag{18}$$

The algorithm for designing the standard Oustaloup filter can be summarized from the above equations.

However, because the above filter algorithm does not fit well at the frequency boundaries w_b, w_h, and the numerator and denominator are of the same order, and the transfer function is not a strictly regular system, the following mathematical model is proposed to improve the standard Oustaloup filter.

$$s^{\gamma} \approx \left(\frac{dw_h}{b}\right)^{\gamma}\left(\frac{ds^2+bw_hs}{d(1-\gamma)s^2+bw_hs+d\gamma}\right)\prod_{k=1}^{N}\frac{s+w_k'}{s+w_k} \tag{19}$$

where,

$$w_k' = w_b {w_u}^{(2k-1-\gamma)/N} \tag{20}$$

$$w_k = w_b {w_u}^{(2k-1+\gamma)/N} \tag{21}$$

$$K = w_h^{\gamma} \tag{22}$$

From the above filter model, it can be seen that the order of the fractional order operator satisfies $\gamma\epsilon(0,1)$. Typically, the weighting parameters are taken to be $b = 10$ and $d = 9$.

After writing the programs, a sine function is used to verify the accuracy of the above model. The fractional order is taken as 0.5, the filter order is taken as 5, and the frequency band is taken as $[0.01,\ 1000]$. Two sine functions are used with $\omega = 1$ and $\omega = 100\pi$, respectively, for the simulation test. The fitting curves of the definition methods and filter methods are shown in Figure 9.

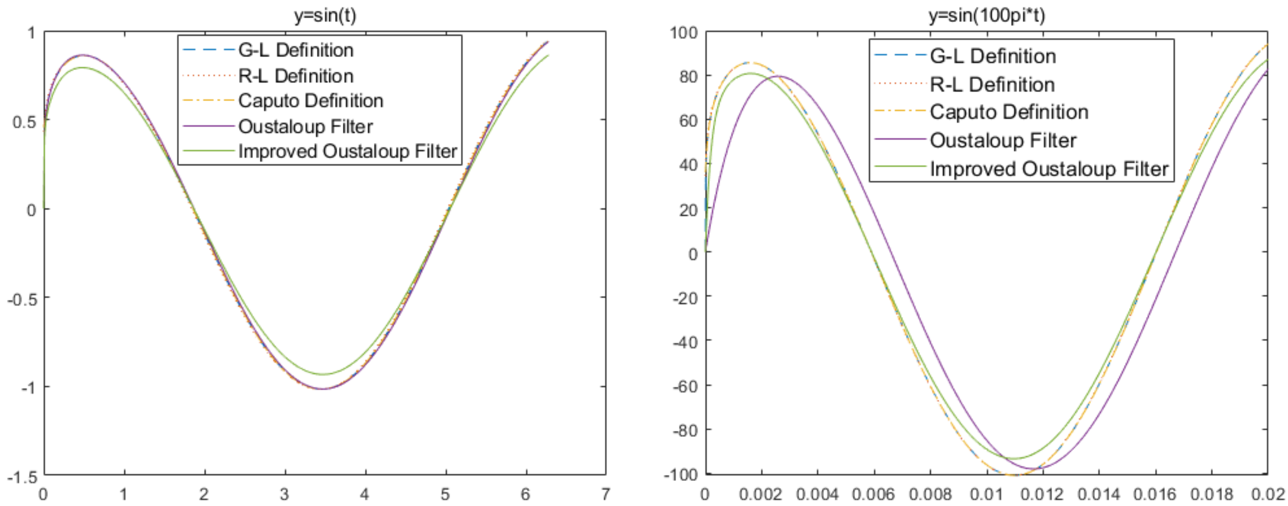

Figure 9. Fitting curves of definition methods and filter methods.

In order to analyze the results easily, the fitting curves were amplified as shown in Figure 10.

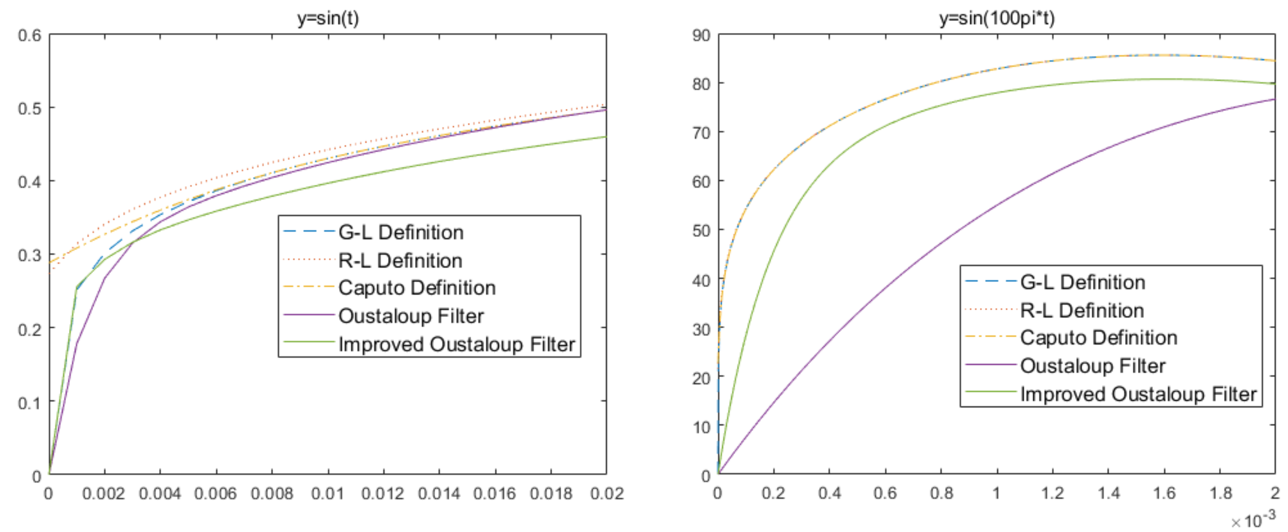

Figure 10. Amplified fitting curves of definition methods and filter methods.

As shown in Figures 9 and 10, the fitting results of the Oustaloup filter and improved Oustaloup filter in the low-frequency range are basically consistent with the definition methods. In the high-frequency range, the fitting results of the improved Oustaloup filter are better than those of the Oustaloup filter, which proves the accuracy of the improved Oustaloup filter.

In order to make the curves smooth, prevent the algebraic loops in the system and improve the computational performance, a low-pass filter is added after the improved Oustaloup filter.

The low-pass filter should optimize the performance of the simulation system and cannot affect the calculation accuracy. Based on the existing research and simulation experiment, the filter has the best performance when the low-pass filter is chosen as $\frac{1}{0.001s+1}$. The fitting curves under four harmonic components are shown in Figure 11.

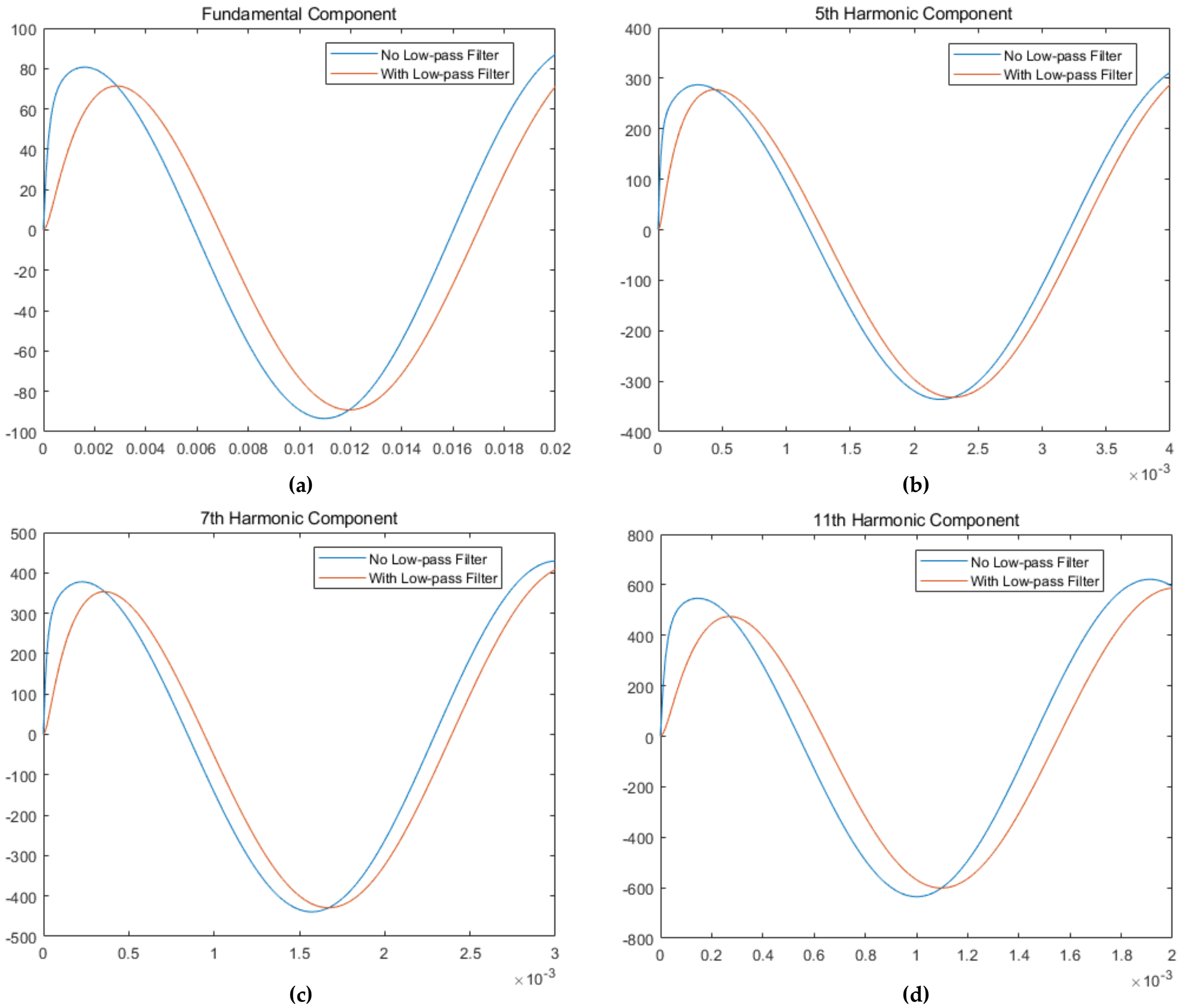

Figure 11. Fitting curves with low-pass filter under different harmonic components: (**a**) fitting curves of fundamental component, (**b**) fitting curves of 5th harmonic component, (**c**) fitting curves of 7th harmonic component, (**d**) fitting curves of 11th harmonic component.

It can be seen from Figure 11 that by using the low-pass filter, the curves are smoother at the beginning of the simulation under the four operating conditions, and the accuracy of the values is not significantly affected.

In this paper, the improved Oustaloup filter is packaged to freely apply the fractional-order filter algorithm to the circuit model simulation. The whole fractional order operator module based on improved Oustaloup filter is shown in Figure 12.

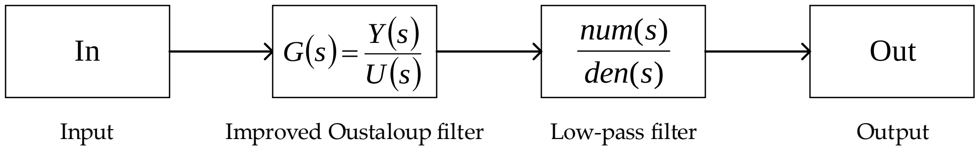

Figure 12. The fractional order operator module based on improved Oustaloup filter.

4.2. Fractional Order Lumped Parameter Circuit Model

With the electrical parameters solved by the simulation model, the lumped parameter equivalent circuit model of the transformer is established as shown in Figures 13 and 14. The model includes series resistance R_h and R_l, series inductance L_h and L_l, coupling capacitance between two adjacent windings C_W, series resistance between two adjacent windings R_W, coupling capacitance between winding and ground of HV and LV windings C_{gh} and C_{gl}, parallel coupling capacitance between HV and LV windings of the same phase C_A, C_B and C_C, parallel coupling capacitance between adjacent HV windings C_{AB} and C_{BC}, mutual inductance between HV and LV windings of the same phase M_A, M_B and M_C, mutual inductance between different HV windings M_{AB}, M_{AC} and M_{BC}, and mutual inductance between different LV windings M_{ab}, M_{ac} and M_{bc}. The transformer is connected as a YND11 connection. The actual power frequency sinusoidal AC supplies U_A, U_B, U_C are on the primary side and the load resistors R_1, R_2, R_3 are on the secondary side.

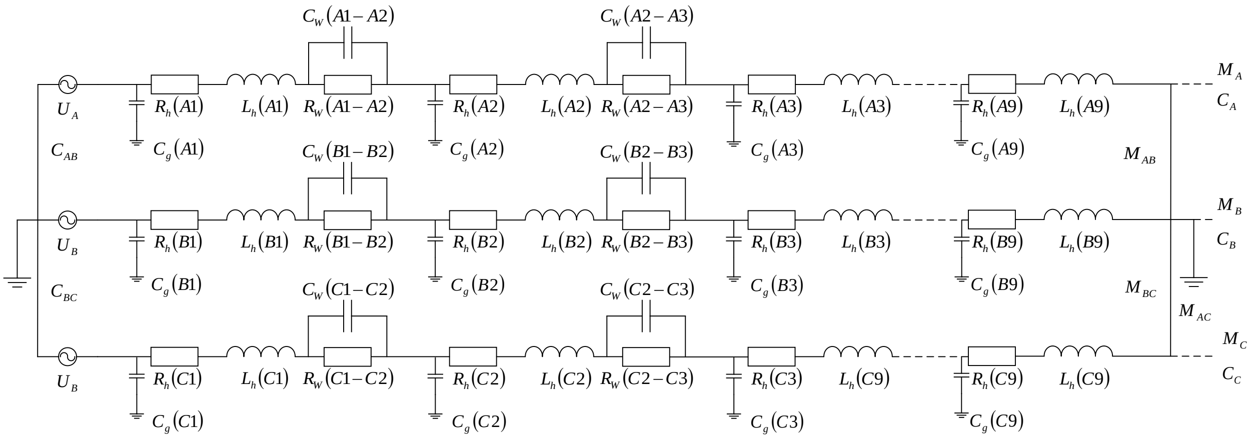

Figure 13. Lumped parameter equivalent circuit model of high-voltage winding.

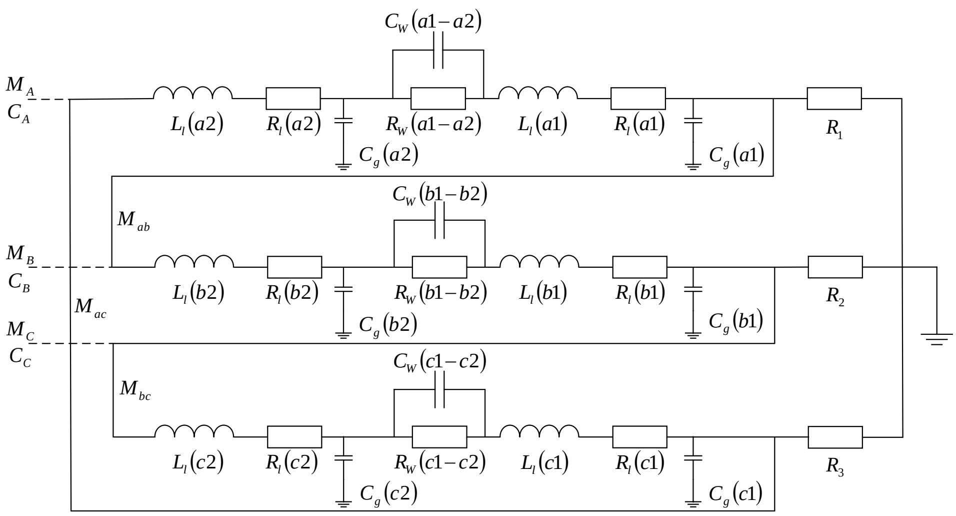

Figure 14. Lumped parameter equivalent circuit model of low-voltage winding.

5. Fractional Order Numerical Calculation

Under rated operating conditions, the electromagnetic forces in transformer windings are subjected to two forces: the radial electromagnetic force, and the axial electromagnetic force. The radial electromagnetic force is along the coil radius, the inner and the outer windings of the current direction are opposite, so that the inner coils bear the inward force, and the outer coils bear the outward force. The axial electromagnetic force is along the coil axis, and the coils also bear inward or outward force. When the transformer works under a short-circuit fault, if the short-circuit electromagnetic force is large enough, the winding will deform due to insufficient capability to resist short-circuit dynamic force. Therefore, when a transformer fault occurs, the magnitude and distribution of the electromagnetic forces in the winding will change. The electromagnetic force of a winding is an important indicator for monitoring the operating conditions of the transformer.

Accurate calculation of the electromagnetic forces provides a reliable assessment of the operating conditions of the transformer. According to the Lorentz law, the electromagnetic forces on the windings can be calculated by Equation (23).

$$F = NBIL \tag{23}$$

where F is the electromagnetic force of a winding, N is the number of turns of coil in the winding, B is the magnetic leakage density, I is the current in the winding, and L is the length of wire in the winding.

5.1. Fractional Order Currents

To calculate the electromagnetic force, the winding current must be calculated. In the traditional circuit model, the current is expressed as:

$$I = \frac{U}{Z} + C\frac{dU}{dt} \tag{24}$$

where I is the integer order winding current, U is the supply voltage, Z is the impedance of the winding, and C is the equivalent capacitance of the winding.

In the fractional order circuit model, the fractional-order capacitance is used instead of the integer-order capacitance, and the integer-order differentiation is changed to fractional-order differentiation by using the fractional-order differentiation operator. The expression is shown in Equation (25).

$$I_\alpha = \frac{U}{Z} + C_\alpha\frac{d^\alpha U}{dt} \tag{25}$$

where I_α is the fractional order winding current, and C_α is the fractional order equivalent capacitance of the winding.

Take the A-phase winding as the example for calculation. Based on the lumped parameter equivalent circuit model, the fractional-order current expressions for the high-voltage winding and low-voltage winding of phase A are shown as follows.

$$\begin{aligned} I_{AH} = \tfrac{U_A}{Z_A} + \sum_{k=1}^{8} C_{wA}\frac{d^\alpha\left(U_{A(k+1)} - U_{A(k)}\right)}{dt} + \sum_{i=1}^{2}\sum_{k=1}^{9} C_{ai(k)}\frac{d^\alpha\left(U_{A(k)} - U_{a(i)}\right)}{dt} \\ - \sum_{i=1}^{9}\sum_{k=1}^{9} C_{AB(ik)}\frac{d^\alpha\left(U_{A(i)} - U_{B(k)}\right)}{dt} - \sum_{k=1}^{9} C_{g(k)}\frac{d^\alpha\left(U_A - U_{A(k-1)}\right)}{dt} \end{aligned} \tag{26}$$

$$I_{AL} = \frac{U_a}{Z_a} + C_{wa}\frac{d^\alpha\left(U_{a(1)} - U_{a(2)}\right)}{dt} - \sum_{i=1}^{2}\sum_{k=1}^{9} C_{ai(k)}\frac{d^\alpha\left(U_{A(k)} - U_{a(i)}\right)}{dt} - \sum_{i=1}^{2} C_{g(k)}\frac{d^\alpha\left(U_a - U_{a(k-1)}\right)}{dt} \tag{27}$$

where I_{AH} is the high-voltage winding current, I_{AL} is the low-voltage winding current, Z_A is the impedance of the high-voltage winding of phase A, Z_a is the impedance of the low-voltage winding of phase A, $U_{(Ak)}$ is the potential of each segment of the high-voltage winding of phase A, $U_{(Bk)}$ is the potential of each segment of the high-voltage winding of phase B, $U_{(ak)}$ is the potential of each segment of the low-voltage winding of phase A, C_{wA} is the coupling capacitance between two adjacent series high-voltage windings of phase A, C_{wa} is the coupling capacitance between two adjacent series low-voltage windings of phase A, C_a is the coupling capacitance between the high-voltage windings and the low-voltage windings of phase A, C_{AB} is the coupling capacitance between the high-voltage windings of phase A and the high-voltage windings of phase B, C_g is the coupling capacitance between the windings and ground, and α is the fractional order.

At present, studies on fractional order capacitance mostly use the integer order to approximate fractional order, but there is still no clearer unified standard for obtaining the order. In this paper, 0.8 order is used as the reference value, the 0.02 order step is taken based on the reference value for simulation calculation, and the actual calculation results are more consistent with the transformer rated value when the fractional order is taken as 0.9. Therefore, the calculation in this paper is performed on the basis of 0.9 order.

Use finite element method to calculate the integer order current of the transformer winding and numerical method to calculate the fractional order current of the transformer winding. Taking the A-phase winding as the example, the fractional order current waveforms of the A phase high-voltage and low-voltage windings under the rated operating conditions are obtained as shown in Figure 15.

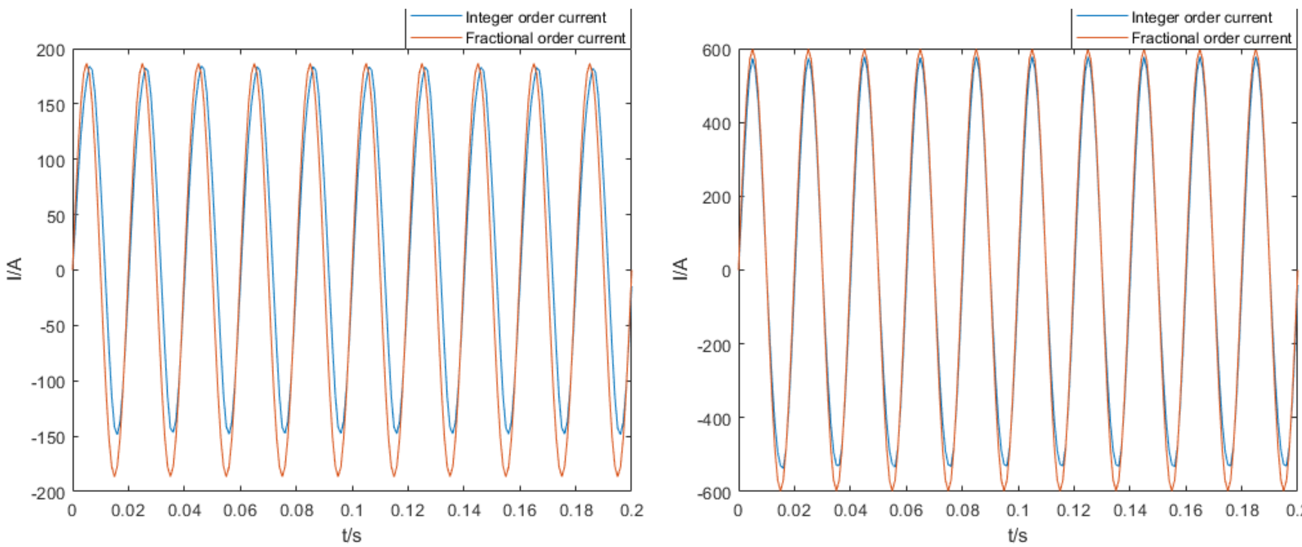

(a) A-phase high voltage winding current

(b) A-phase low voltage winding current

Figure 15. Waveforms of A-phase winding currents.

To analyze the results easily, the current waveforms were amplified within one period as shown in Figure 16.

The rated amplitude value of the phase current of the high-voltage winding is 186.6762 A, and the rated amplitude value of the phase current of the low-voltage winding is 598.492 A. The simulation results show that in the positive half period, the values of fractional current and integer current are close, and the values of fractional current are higher and closer to the rated values. In the negative half period, the amplitude values of integer order phase current of the high-voltage winding and low-voltage winding are both significantly smaller than the rated values, and the waveforms of the integer order current are not the strictly sinusoidal waves. The results for the integer order current are not correct in the negative half period mainly because of the systematic error of the finite element method. The fractional order current is the standard sinusoidal wave, and the values are closer to the rated values. The simulation results for the fractional order model are more accurate than those for the integer order model.

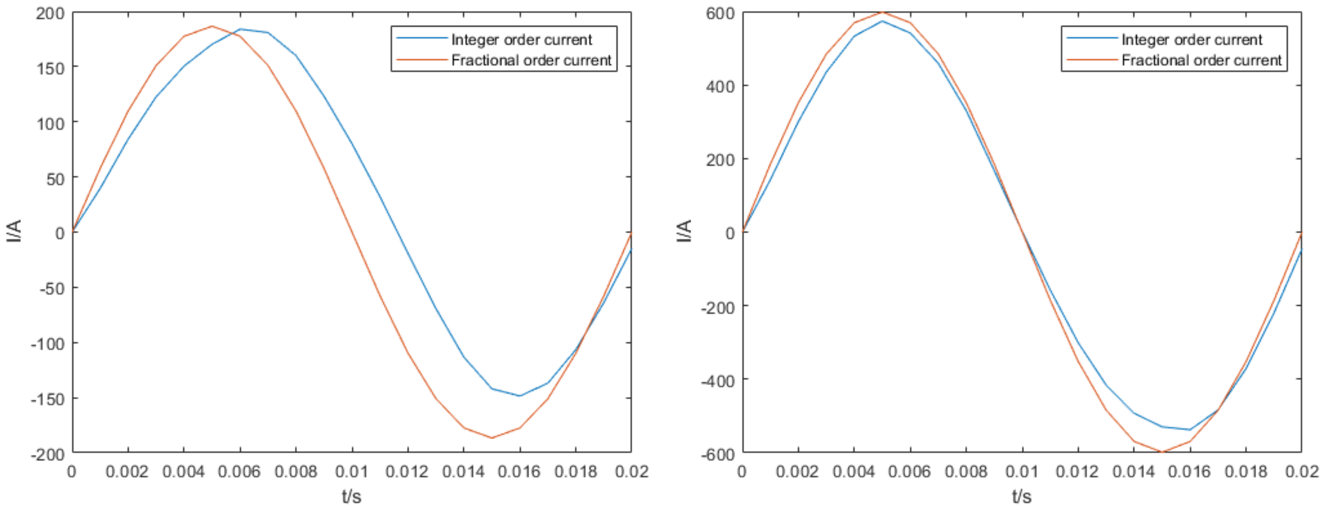

(a) A-phase high voltage winding current **(b)** A-phase low voltage winding current

Figure 16. Amplified waveforms of A-phase winding currents within one period.

To further verify the accuracy of the fractional order model, the amplitude value of the secondary phase current was calculated for five different operating conditions: 50% load rate, 80% load rate, 100% load rate, 150% load rate and 200% load rate. The results are shown in Table 5.

Table 5. The amplitude value of phase current on the secondary side at different load rates.

Operating Mode	Load Rates				
	0.5	0.8	1.0	1.5	2.0
Rated value/A	299.246	478.7936	598.492	897.738	1196.984
Fractional order value/A	295.3842	472.6173	590.7715	886.1566	1181.5418
Error	1.29%	1.29%	1.29%	1.29%	1.29%
Integer order value/A	293.8825	467.8946	584.6302	849.9375	1107.1758
Error	1.79%	2.28%	2.32%	5.32%	7.50%

As the load ratios increase, the calculation errors of the integer order simulation model become larger and larger. The calculation results are more accurate using the 0.9 order fractional order model.

Compare the above calculation results with existing research results to verify the accuracy of the fractional order model. The errors of the current on the secondary side at different load rates studied by paper [25] are shown in Table 6.

Table 6. The errors of the current on the secondary side at different load rates [25].

Operating Mode	Load Rates						
	0.2	0.4	0.6	0.8	1.0	1.2	1.4
Error	1.74%	3.35%	2.35%	2.36%	2.93%	2.88%	3.18%

By comparing the error values, the fractional order model proposed in this paper is shown to be more accurate than the finite element model.

5.2. Fractional Order Electromagnetic Forces

Equation (23) is modified to give the expression for the fractional order electromagnetic force:

$$F_\alpha = NI_\alpha \pi(r_1 + r_2)\int_V dB \tag{28}$$

where F_α is the fractional order electromagnetic force, I_α is the fractional order current, N is the number of turns of the coil, B is the magnitude of the magnetic flux density, and r_1, r_2 are the inner radius and outer radius of the winding, respectively.

After obtaining the magnitude of the magnetic flux density by Equation (4) and the fractional order current by Equation (25), the field-circuit coupling method is applied to solve for the fractional-order electromagnetic forces in the windings, as shown in Figure 17.

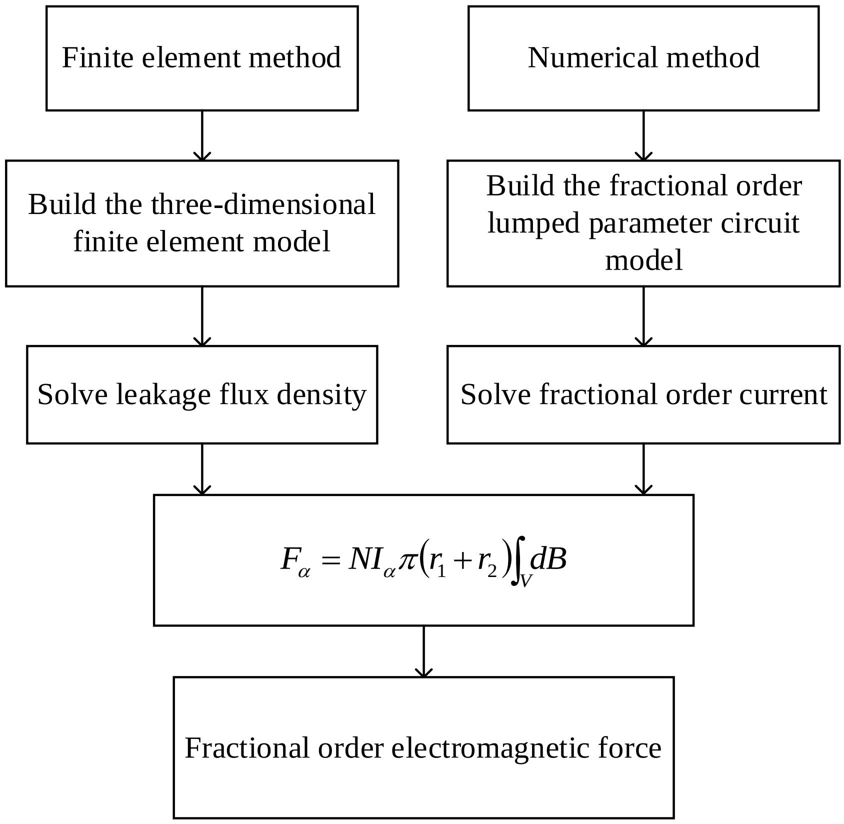

Figure 17. Schematic diagram of field-circuit coupling.

The integer order and fractional order electromagnetic forces in the A-phase winding under rated operating conditions are shown in Figure 18.

The waveform is amplified for convenient observation and analysis as shown in Figure 19.

It can be seen that the maximum electromagnetic force of the high-voltage winding under normal conditions is around 105 newtons, and the maximum electromagnetic force of the low-voltage winding under normal conditions is around 62 newtons. The fractional order model is simpler, the calculation results are more accurate, and the running time of the program is shorter.

Three-phase short-circuit faults are the most serious faults in transformers. Inadequate short-circuit resistance of the winding is prone to cause winding deformation and, in severe cases, line tripping or even explosion and burning. Simulations have been carried out to calculate the fractional and integer order current and electromagnetic forces in three-phase short-circuited working conditions. The currents and electromagnetic forces are shown in Figures 20 and 21.

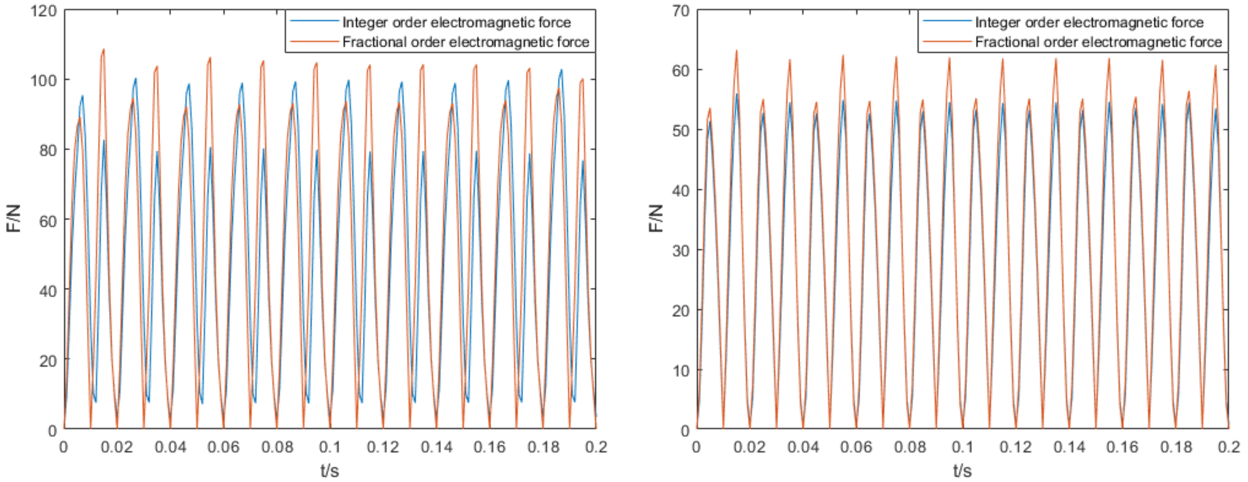

(a) A-phase high voltage winding electromagnetic force **(b)** A-phase low voltage winding electromagnetic force

Figure 18. Waveform of A-phase winding electromagnetic forces.

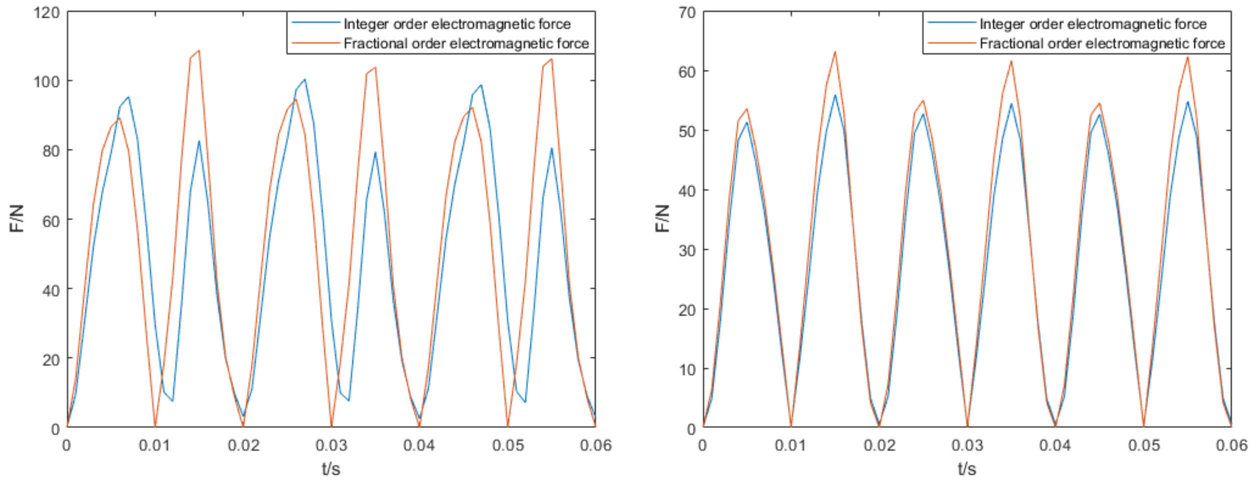

(a) A-phase high voltage winding electromagnetic force **(b)** A-phase low voltage winding electromagnetic force

Figure 19. Waveform of A-phase winding electromagnetic forces.

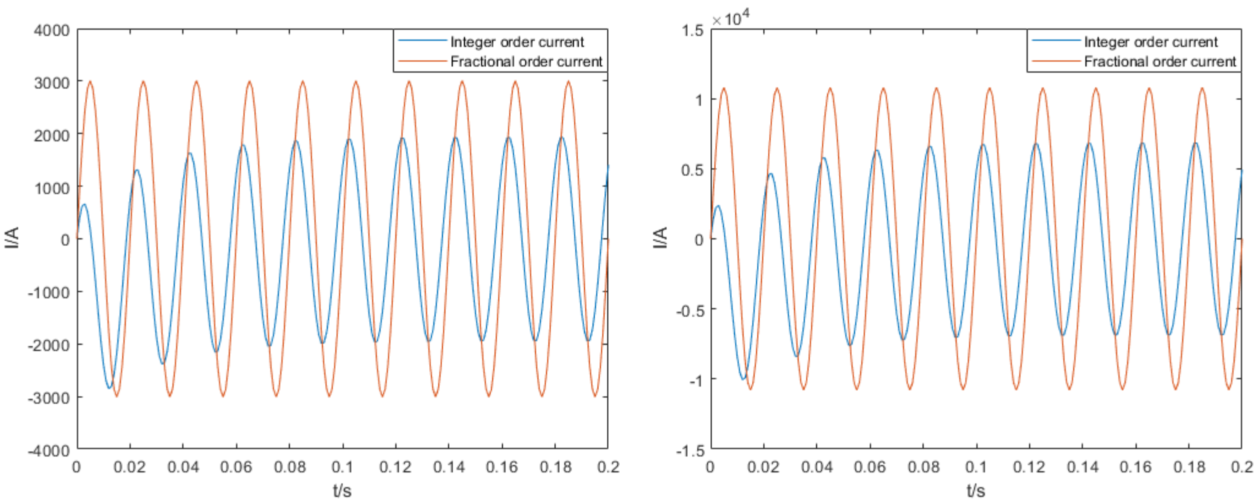

(a) A-phase high voltage winding current **(b)** A-phase low voltage winding current

Figure 20. Waveforms of A-phase winding currents under three-phase short circuit.

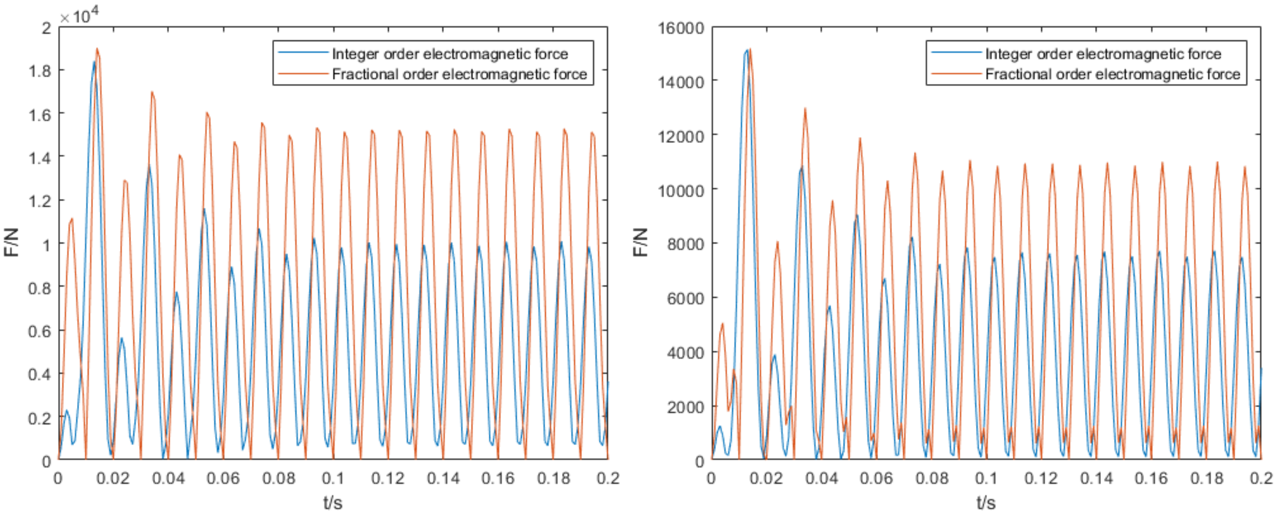

(a) A-phase high voltage winding electromagnetic force **(b)** A-phase low voltage winding electromagnetic force

Figure 21. Waveforms of A-phase winding electromagnetic forces under three-phase short circuit.

The waveform is amplified for convenient observation and analysis as shown in Figure 22.

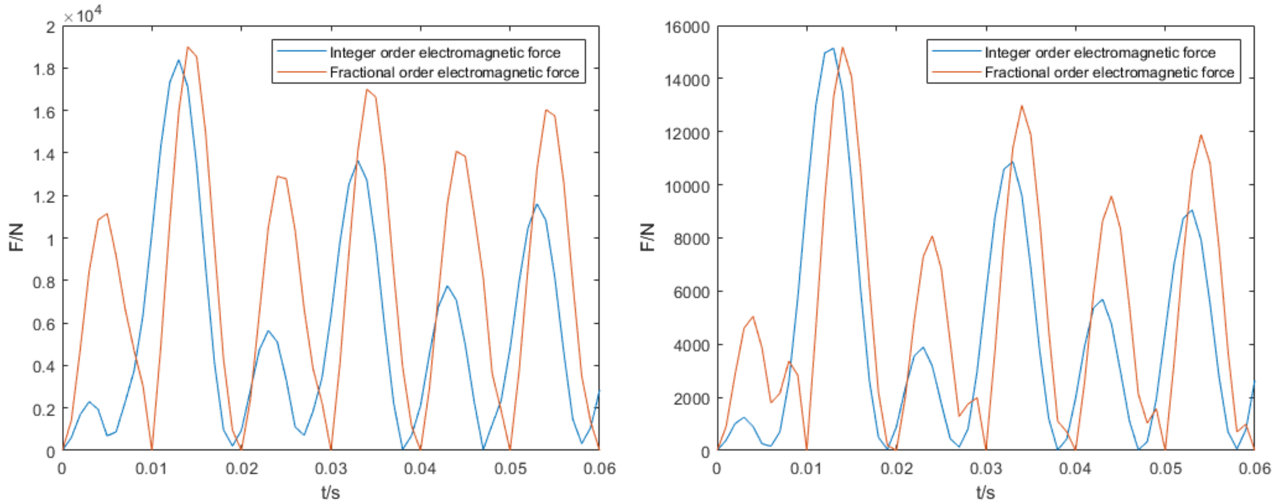

(a) A-phase high voltage winding electromagnetic force **(b)** A-phase low voltage winding electromagnetic force

Figure 22. Waveform of A-phase winding electromagnetic forces.

The figures show that the maximum short-circuit impulse current of the A-phase high-voltage winding under three-phase short-circuit conditions is 10 kA, the maximum short-circuit impulse current of the low-voltage winding is 3 kA, and the electromagnetic force applied to the winding reaches more than 14,000 N, which seriously endangers the operational safety of the transformer, which should be removed from operation in time before power failure.

Compare the above values with existing research results to verify the accuracy of the fractional order model. Authors of [26] used the same transformer model as described in this paper and determined that under three-phase short-circuit conditions, the electromagnetic force of the high-voltage winding is about 14,000 N, and the electromagnetic force of the low-voltage winding is about 10,000 N. Similarly to the results obtained with the finite element method, the calculation results obtained by [26] were smaller than those obtained with the fractional order model. If the transformer is designed based on inaccurate calculation results, it may be damaged because of insufficient mechanical strength when working under exceptional conditions. By accurately calculating the winding force, the operating state of the winding ground can be reliably determined to avoid causing instability of the power system.

The transformer proposed in this paper is used in an offshore wind power platform. The offshore wind power system contains a large number of powered electronic devices, which may lead to an increase in the harmonic components in the power system. The effect of harmonic voltage and harmonic current on the transformer should be considered to obtain the accurate electromagnetic force in the windings. The forces on the fractional and integer orders of the A-phase winding in the 5th, 7th and 11th harmonic cases were simulated and analyzed. The electromagnetic forces are shown in Figure 23.

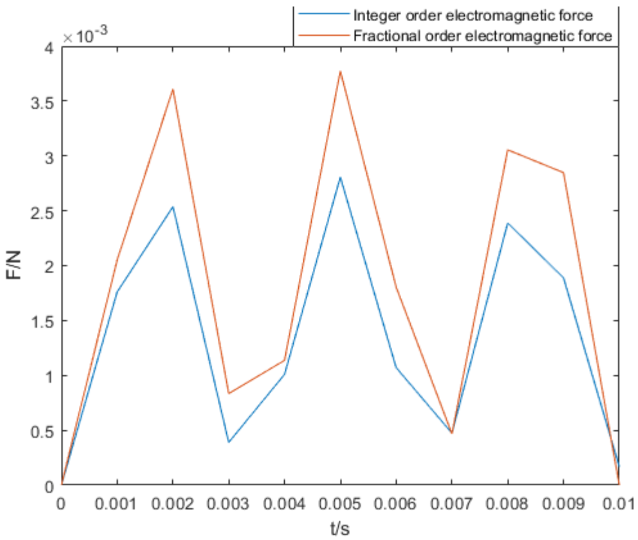

(a) A-phase high voltage winding electromagnetic force

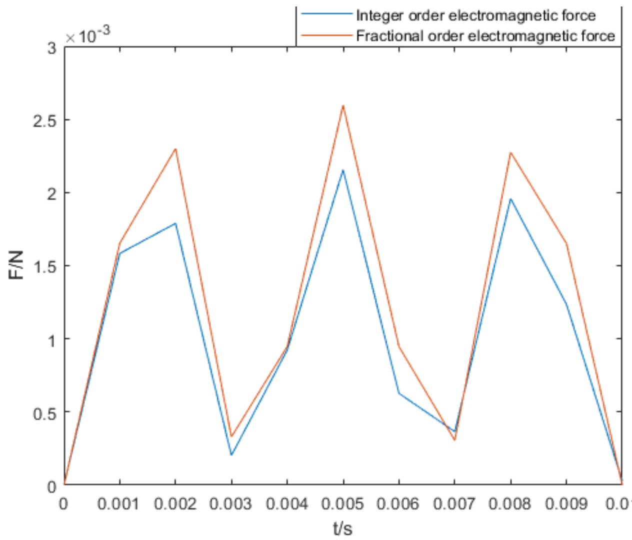

(b) A-phase low voltage winding electromagnetic force

Figure 23. Waveforms of A-phase winding harmonic electromagnetic forces.

Accompanying the presence of harmonics, the winding current will be disturbed within a certain scope. Although the transient value of the electromagnetic force does not exceed a limited value, prolonged operation in a harmonic environment may lead to overload and overheating, which would seriously damage the equipment. Therefore, it is essential to eliminate harmonics in time.

6. Conclusions

Nowadays, accurate calculations of the electromagnetic force in transformer windings not only facilitate the expected design and provide guidelines for transformer design, they also help the power sector to improve the reliability of equipment condition assessments and schedule reasonable maintenance time. In existing study methods, the errors of finite element simulations are large and consume more computing time, and the actual parameters of components are not reflected accurately with the integer order model. To address these problems, in this paper, model simulations are carried out for a dry-type offshore wind power transformer, the electrical parameters of the transformer are calculated by the finite element method, and the fractional order lumped parameter equivalent circuit model of a transformer is proposed. The current and electromagnetic force of the winding under different operating conditions are calculated. Based on the simulation and analysis of the experimental results, the following conclusions are derived.

1. A fractional-order differential operator with the improved Oustaloup filter is built to replace the integer order capacitance, and the results show that the calculation of the transformer winding current at the 0.9 order is more consistent with the rated values than at the integer order. The integer order current is not the standard sinusoidal

wave, and the error is significant in the negative half period compared to the rated value. The 0.9 order circuit model can describe the actual characteristics of circuit components more accurately;
2. The fractional order lumped parameter equivalent circuit model is established, and the fractional order winding current calculation method is proposed for the offshore wind power transformer under different load rates. Compared with the integer order current model, the fractional order model is more accurate and imposes low computational expense, and the calculation results are more accurate and reliable;
3. Based on field-circuit coupling, the fractional order electromagnetic force calculation method is proposed. By applying the fractional-order circuit model to simulate the electromagnetic force under different operating conditions, the results verify the correctness of the fractional-order model. The fractional order lumped parameter equivalent circuit model proposed in this paper can calculate the electromagnetic forces of windings under different operating conditions such as different load rates, short circuits, harmonics, etc.
4. Comparing the integer order results with the fractional order results, the integer order results are smaller than the fractional order results and have a significant deviation from the rated value. Using the integer order calculation method to monitor the operation of a transformer may lead the transformer to operate under overload conditions for a long time, which can accelerate insulation aging and accumulation of deformation faults. The fractional order model improves the reliability and accuracy of transformer structural design. Accurate electromagnetic force analysis can improve the reliability of the equipment condition assessment and prevent the occurrence of winding deformation faults.

The significance of this paper is reflected in two aspects. Firstly, the fractional order characteristics of circuit components are well described by using a fractional order filter, which is fitter than integer order with the actual situation of nature. Secondly, the fractional order lumped parameter equivalent circuit model is established to realize the accurate and fast calculation of the electromagnetic force. Although the model proposed in this paper is based on an offshore transformer, the method proposed in this paper is equally suitable for any onshore dry-type transformer. In subsequent research, the relationship between the structural parameters and fractional order electromagnetic force will be considered to analyze winding deformation faults, and the fractional order electromagnetic force, thermal stress, and vibration mode will be systematically combined to realize accurate online monitoring of transformers and further guide the operation and service life prediction of transformers.

Author Contributions: Conceptualization, H.Z. and Y.Z.; methodology, Y.Z.; software, Y.Z.; validation, R.W. and X.O.; formal analysis, H.Z. and Y.Z.; investigation, Y.Z., R.W. and X.O.; resources, H.Z. and L.Z.; writing—original draft preparation, Y.Z.; writing—review and editing, H.Z. and Y.Z. All authors have read and agreed to the published version of the manuscript.

Funding: This work was supported by the Shandong Province Key Research and Development Plan (Project number: 2021CXGC010210) and the Natural Science Foundation of Shandong Province (Grant No. ZR2020ME203).

Data Availability Statement: Not applicable.

Conflicts of Interest: The authors declare no conflict of interest.

References

1. Pan, C.; Wang, C.; Liu, Z.; Chen, X. Winding vibration analysis of unbalanced transformer based on electromagnetic-mechanical coupling. *Int. J. Electr. Power Energy Syst.* **2022**, *134*, 107459. [CrossRef]
2. Soloot, A.H.; Høidalen, H.K.; Gustavsen, B. Influence of the winding design of wind turbine transformers for resonant overvoltage vulnerability. *IEEE Trans. Dielectr. Electr. Insul.* **2015**, *22*, 1250–1257. [CrossRef]
3. Tenbohlen, S.; Jagers, J.; Gebauer, J.; Müller, P.; Lapworth, J.; Yukiyasu, S.; Desai, B.; McIntosh, A.; Bastos, G.; Bo, L. Transformer Reliability Survey: Interim Report. *Electra* **2012**, *261*, 46–49.

4. Dai, L.; Wang, H.; Qin, Y.; Shi, G.; Zhang, J.; Cai, X. Analysis and Suppression of High-Frequency Resonance for Offshore Wind Power Grid-Connected Converter Considering Cable Capacitance Effect. *Electronics* **2023**, *12*, 2638. [CrossRef]
5. Gao, S.; Sun, L.; Liu, H. Calculation of axial electromagnetic force of transformer under short circuit condition based on COMSOL multi-physical field simulation. *Sci. Technol. Eng.* **2022**, *22*, 5250–5256.
6. Nezhad, A.E.; Samimi, M.H. Power Transformer Vibration Study and its Application in Winding Deformation Detection. In Proceedings of the 30th International Conference on Electrical Engineering, Seoul, Republic of Korea, 28 June–2 July 2022; pp. 320–324.
7. Wang, J.; Xing, Y.; Ma, X.; Zhao, Z.; Yang, L. Numerical Investigations for Vibration and Deformation of Power Transformer Windings under Short-Circuit Condition. *Energies* **2023**, *16*, 5318. [CrossRef]
8. Li, Y.; Xu, Q.; Lu, Y. Electromagnetic Force Analysis of a Power Transformer Under the Short-Circuit Condition. *IEEE Trans. Appl. Supercond.* **2021**, *31*, 0603803. [CrossRef]
9. Zhou, L.; Zhou, X.; Wu, Z.; Lin, T.; Xu, X.; Zhang, C. Modeling of Oscillating Waves in Transformer Windings and Analysis of Axial Shift Faults. *Electr. Power Autom. Equip.* **2021**, *41*, 157–163.
10. Ding, Q.; Yao, Y.; Wang, B.; Fu, J.; Zhang, W.; Zeng, C.; Li, X.; Valtchev, S.A. Modified Lumped Parameter Model of Distribution Transformer Winding. *Glob. Energy Interconnect.* **2020**, *3*, 158–165. [CrossRef]
11. Li, F.; Zhang, Y.; Xu, J.; Zhu, M.; Zhang, C. Simulation Research on Sweep Frequency Impedance Characteristics of Transformer Winding Based on Three-Phase Three-Winding Lumped Parameter Model. In Proceedings of the 2020 IEEE International Conference on High Voltage Engineering and Application, Beijing, China, 6–10 September 2020; pp. 1–4.
12. Bohannan, G.W. Analog Realization of a Fractional Control Element—Revisited. In Proceedings of the 41st IEEE International Conference on Decision and Control, Tutorial Workshop 2: Fractional Calculus Applications in Automatic Control and Robotics, Las Vegas, NV, USA, 10–13 December 2002; p. 1.
13. Jonscher, A.K. Dielectric Relaxation in Solids. *J. Phys. D Appl. Phys.* **1999**, *32*, 57–70. [CrossRef]
14. Srivastava, H.; Aouf, M. A Certain Fractional Derivative Operator and Its Applications to a New Class of Analytic and Multivalent Functions with Negative Coefficients. *J. Math. Anal. Appl.* **1992**, *171*, 1–13. [CrossRef]
15. Westerlund, S.; Ekstam, L. Capacitor theory. *IEEE Trans. Dielectr. Electr. Insul.* **1994**, *1*, 826–839. [CrossRef]
16. Tseng, C.-C.; Lee, S.-L. Fractional Derivative Constrained Design of FIR Filter with Prescribed Magnitude and Phase Responses. In Proceedings of the 2013 European Conference on Circuit Theory and Design, Dresden, Germany, 8–12 September 2013; pp. 1–4.
17. Liang, G.; Zhang, J. Research on Passive Synthesis Method of Four-component Fractional-order Circuit. *J. North China Electr. Power Univ.* **2021**, *48*, 73–81.
18. Piotrowska, E.; Sajewski, Ł. Analysis of an Electrical Circuit Using Two-Parameter Conformable Operator in the Caputo Sense. *Symmetry* **2021**, *13*, 771. [CrossRef]
19. Liao, K.; Lu, D.; Wang, M.; Yang, J. A Low-Pass Virtual Filter for Output Power Smoothing of Wind Energy Conversion Systems. *IEEE Trans. Ind. Electron.* **2022**, *69*, 12874–12885. [CrossRef]
20. Guha, D.; Roy, P.K.; Banerjee, S. Adaptive fractional-order sliding-mode disturbance observer-based robust theoretical frequency controller applied to hybrid wind–diesel power system. *ISA Trans.* **2023**, *133*, 160–183. [CrossRef] [PubMed]
21. Liu, L.; Zhang, S.; Zhang, L.; Pan, G.; Yu, J. Multi-UUV Maneuvering Counter-Game for Dynamic Target Scenario Based on Fractional-Order Recurrent Neural Network. *IEEE Trans. Cybern.* **2023**, *53*, 4015–4028. [CrossRef] [PubMed]
22. Sun, Y.; Xu, G.; Li, N.; Li, K.; Liang, Y.; Zhong, H.; Zhang, L.; Liu, P. Hotspot Temperature Prediction of Dry-Type Transformers Based on Particle Filter Optimization with Support Vector Regression. *Symmetry* **2021**, *13*, 1320. [CrossRef]
23. Zhou, L.; Jiang, J.; Li, W.; Wu, Z.; Gao, S.; Guo, L.; Liu, H. FRA Modelling for Diagnosing Axial Displacement of Windings in Traction Transformers. *IET Electr. Power Appl.* **2019**, *13*, 2121–2127. [CrossRef]
24. Oustaloup, A.; Levron, F.; Mathieu, B.; Nanot, F.M. Frequency-band complex noninteger differentiator: Characterization and synthesis. *IEEE Trans. Circuits Syst. I Fundam. Theory Appl.* **2000**, *47*, 25–39. [CrossRef]
25. Li, N.; Sun, Y.; Hu, Y.; Zhang, L.; Zhong, H.; Wang, E. The Temperature Variation Characteristic Analysis Based on the Electromagnetic Thermal Coupled Method for the Dry-type Transformer. In Proceedings of the 2019 22nd International Conference on Electrical Machines and Systems, Harbin, China, 11–14 August 2019; pp. 1–5.
26. Wang, E.; Sun, Y.; Zhong, H.; Xie, X.; Li, N.; Hu, Y.; Zhang, L. Modal Analysis for the Vibration of the Dry-Type Transformer in the Offshore Oil Exploitation Power System. In Proceedings of the 2019 IEEE Sustainable Power and Energy Conference, Beijing, China, 21–23 November 2019; pp. 2008–2013.